An Energy Tank-Based Interactive Control Architecture for Autonomous and Teleoperated Robotic Surgery

Federica Ferraguti, *Member, IEEE*, Nicola Preda, Auralius Manurung, *Student Member, IEEE*, Marcello Bonfè, *Member, IEEE*, Olivier Lambercy, *Member, IEEE*, Roger Gassert, *Senior Member, IEEE*, Riccardo Muradore, *Member, IEEE*, Paolo Fiorini, *Fellow, IEEE*, and Cristian Secchi, *Member, IEEE*

***Abstract*—Introducing some form of autonomy in robotic surgery is being considered by the medical community to better exploit the potential of robots in the operating room. However, significant technological steps have to occur before even the smallest autonomous task is ready to be presented to the regulatory authorities. In this paper, we address the initial steps of this process, in particular the development of control concepts satisfying the basic safety requirements of robotic surgery, i.e., providing the robot with the necessary dexterity and a stable and smooth behavior of the surgical tool. Two specific situations are considered: the automatic adaptation to changing tissue stiffness and the transition from autonomous to teleoperated mode. These situations replicate real-life cases when the surgeon adapts the stiffness of her/his arm to penetrate tissues of different consistency and when, due to an unexpected event, the surgeon has to take over the control of the surgical robot. To address the first case, we propose a passivity-based interactive control architecture that allows us to implement stable time-varying interactive behaviors. For the second case, we present a two-layered bilateral control architecture that ensures a stable behavior during the transition between autonomy and teleoperation and, after the switch, limits the effect of initial mismatch between master and slave poses. The proposed solutions are validated in the realistic surgical scenario developed within the EU-funded I-SUR project, using a surgical robot prototype specifically designed for the autonomous execution of surgical tasks like the insertion of needles into the human body.**

***Index Terms*—Energy tanks, interactive control, medical robots and systems, telerobotics.**

Manuscript received July 23, 2014; revised March 31, 2015 and May 28, 2015; accepted July 9, 2015. Date of publication August 5, 2015; date of current version September 30, 2015. This paper was recommended for publication by Associate Editor R. J. Webster III and Editor B. J. Nelson upon evaluation of the reviewers' comments. This work was supported by the European Union Seventh Framework Programme FP7/2007-2013 under Grant 270396 (I-SUR).

F. Ferraguti and C. Secchi are with the Department of Sciences and Methods for Engineering, University of Modena and Reggio Emilia, 41100 Modena, Italy (e-mail: federica.ferraguti@unimore.it; cristian.secchi@unimore.it).

N. Preda and M. Bonfè are with the Engineering Department, University of Ferrara, 44121 Ferrara, Italy (e-mail: nicola.preda@unife.it; marcello.bonfe@unife.it).

A. Manurung, O. Lambercy, and R. Gassert are with the Rehabilitation Engineering Laboratory, ETH Zurich, 8092 Zürich, Switzerland (e-mail: manuruna@student.ethz.ch; olambercy@ethz.ch; gassertr@ethz.ch).

R. Muradore and P. Fiorini are with the Department of Computer Science, University of Verona 37129 Verona, Italy (e-mail: riccardo.muradore@univr.it; paolo.fiorini@univr.it).

Color versions of one or more of the figures in this paper are available online at http://ieeexplore.ieee.org.

Digital Object Identifier 10.1109/TRO.2015.2455791

I. Introduction

THE field of surgical robotics has undergone a considerable evolution in recent years. Surgical robots that help to overcome the limitations of minimally invasive surgery and enhance the capabilities of the surgeon have been developed. Currently, surgical robotic systems are teleoperated by the surgeon, as is the case for the Da Vinci by Intuitive Surgical [1] and with the DLR MiroSurge [2]. One of the main drawbacks of teleoperated surgical robots is the significant amount of required training efforts and the necessity for the surgeon to manually perform all the surgical tasks necessary for the operation. This can increase the mental workload and the fatigue for executing the operation and, consequently, decrease the concentration in some, possibly crucial, parts of the operation. In order to overcome this drawback, the possibility of automatically executing some surgical tasks by a robotic system is increasingly being investigated, automating this way a few phases of the operation [3].

When autonomously executing a surgical task, a robot faces a very challenging situation. In fact, the environment the robot has to interact with (i.e., the body of the patient) is mostly unknown (only some information can be obtained from preoperative imaging) and usually time varying (deformable or nonhomogeneous). Furthermore, the robot may need to change its interactive behavior online, because the operating conditions change. For example, during a needle insertion task, the robot has to be stiff when penetrating the skin, while it has to behave more softly during the insertion. The fact that each patient is different and that, therefore, it is often not possible to determine a standard pattern for the desired behavior increases the task complexity. Finally, the safety of the patient is always the primary concern. As shown in [4], a safe reactive behavior of the robot to some selected complications can be planned in advance. Nevertheless, in the event of unexpected events taking place, it is necessary to let the surgeon take over the control of the robot to drive it to a safe configuration.

Impedance and admittance control strategies [5] are highly suitable candidates to ensure a stable interaction with unknown environments. They allow the engineer to directly shape the behavior by which the robot interacts with the environment. Unfortunately, standard impedance and admittance control schemes cannot guarantee a stable interaction when time-varying interactive behaviors need to be implemented.

Controlling the robot in teleoperation brings other challenges. Bilateral teleoperation has been proven to be very effective for

allowing a human to drive a remote robot [6], and therefore, it is also a good candidate for allowing the surgeon to take over the control of the robot. Nevertheless, when the surgeon switches the robot from an autonomous mode to a teleoperated mode, there is likely a kinematic mismatch between the pose of the master console and that of the surgical robot (i.e., the slave robot). This mismatch can impose a high workload on the surgeon to mentally compensate the offset and can, therefore, lead to risks for the patient because of unintentional motions transmitted to the robot. Furthermore, by simply switching on standard bilateral controllers (e.g., position–position, position–force [7]) in a mismatched situation, unexpected transients on the slave could be experienced. These problems are highly undesirable because the teleoperated mode is activated during critical situations, and mistakes in the teleoperation can cause severe injury to the patient. While many bilateral teleoperation control strategies ensuring an efficient and stable behavior have been proposed in the literature [7], very few bilateral teleoperation systems exist that are capable of switching between autonomous and teleoperated modes in a stable manner and compensating for kinematic mismatches.

The goal of this paper is to present a passivity-based interactive control architecture that allows one to implement stable time-varying interactive behaviors and transient-free kinematically compensated bilateral teleoperation of a robotic platform. In particular, persistent oscillations and diverging behaviors must be avoided and the reaction time of the system must be as fast as possible, without introducing instability. To achieve this aim, we will exploit the port-Hamiltonian framework [8] for modeling the surgical robotic architecture and the concept of energy tanks [9], [10] that allows us to use the (virtual) energy circulating in the controlled system in a flexible and passivity preserving way. This paper extends [11], where a variable stiffness impedance control was provided, by designing a tank-based admittance control strategy where inertia, stiffness, and damping can all be passively changed. Furthermore, we will extend [10] by exploiting energy tanks not only for implementing a passive coupling between master and slave, but also for implementing a stable switch and position compensation in the transition between autonomous and teleoperated mode. This study is part of the FP7 European research project I-SUR (Intelligent Surgical Robotics) whose goal is to develop general methods for cognitive surgical robots in order to automatically execute surgical actions such as puncturing and suturing, as well as for teleoperation by the surgeon [12]. The proposed control strategies, addressing the mentioned issues related to robotic surgery, will be validated using the surgical robot prototype specifically designed within the I-SUR project.

The main contributions of this paper are as follows.

1) A novel tank-based time-varying admittance controller extending the earlier results of [11], allowing one to adapt the interactive behavior of the robot while preserving passivity.
2) A novel flexible and passivity-based teleoperation architecture that ensures a stable switch between autonomous and teleoperated modes and compensates for the kinematic mismatch between the master and the slave (i.e., the surgical robot).
3) The experimental validation in a needle insertion scenario using the I-SUR robotic surgery platform and a realistic phantom model.

This paper is organized as follows. Section II presents an overview of related works in the fields of interactive control and pose offset compensation in teleoperation. Section III provides some background on port-Hamiltonian systems and energy tanks. Section VI gives a short description of the I-SUR robot. In Section IV, the tank-based variable admittance controller is presented, and in Section V, the teleoperation architecture is described. In Section VII, the experimental results are illustrated. Finally, in Section VIII, the conclusion is drawn.

II. Related Works

The growing interest in reproducing a human-like behavior in many robotic tasks fostered the research in interaction control. In this section, we focus on the works addressing the main problems arising in the considered application: time-varying admittance/impedance parameters of the interactive controller and compensation of the kinematic mismatch when switching to teleoperation.

In particular, a lot of research on impedance and admittance control with variable stiffness has been done. Many researchers have addressed the problem of properly estimating online variable stiffness and damping matrices for the execution of an interactive task with an unknown environment (see, e.g., [13], [14]). The time necessary for reaching a good estimate depends on the collected data as well as on the estimation algorithm, and it is hard to predict it in practical applications. In [15], a teleoperation system for needle insertion is presented. The variable stiffness of the environment is considered, estimated, and exploited for adjusting the force perceived by the user.

Several works consider the problem of developing an impedance controller with a variable stiffness, but they address only particular cases. In [16], a tracking error-dependent variable stiffness impedance controller for parallel link manipulators has been proposed in order to increase the robustness of the controlled system with respect to unknown parameters. The way stiffness can be changed is linked to the tracking error, and in case of external disturbances, the target impedance cannot be achieved.

Iterative and adaptive control strategies have been proposed in order to compensate for disturbances and for guaranteeing a stable interaction even in presence of drastic changes in the environment (see, e.g., [17] and [18]). The apparent stiffness of the robot is adapted in order to match the behavior of human motor control. Nevertheless, in several surgical scenarios, special interactive patterns (e.g., stiffness variations) may be necessary to match the behavior of the surgeon or for coping with the particular structure of the patient's body that is provided by pre- and intraoperative data.

In [19] and [20], an efficient human-like force tracking impedance control scheme with varying stiffness has been developed. However, the stiffness profile depends on the force tracking error and cannot be chosen *a priori*.

[1] http://www.isur.eu/isur

Only a limited amount of works have exploited the concept of variable impedance controllers in surgical robotics. In [21], a variable stiffness controlled manipulator was developed in order to provide insights on the design and control of rehabilitation robots. In [22], a variable impedance control was proposed, allowing the surgeon to cooperate with the robot during the execution of high-accuracy tasks in orthopedic surgery, e.g., drilling and shaping of the femur's head. However, in this approach, several assumptions on the choice of the gain matrices are necessary.

Substantial research studies addressing the transition between autonomous and shared control of a robot and considering the kinematic compensation problem are available in the literature. In [23], a shared control teleoperation architecture, obtained by merging human input and autonomous operations, is provided. However, the input from the operator perturbs the state of the robot and the transition between autonomous and teleoperation modes is not smooth. In [24], a hybrid system allowing to switch between different control modes in a teledrilling system is proposed. Nevertheless, when switching from one mode to the other, master and slave have to wait for being synchronized, and this results in a slowly reacting system. In [25], the operation modes for cooperation between manual operation and autonomous functions in intelligent teleoperation systems are discussed. In [26], Xiong *et al.* describe other operation modes and discuss the case of time delay. These works are mainly related to the way the operator can change the operation modes intuitively and smoothly. They do not address the problem of compensating the position error arising between master and slave when the system switches between different modes.

Several works have addressed the problem of position offset compensation. In [27], a strategy to passively compensate the steady-state position error due to packet loss is proposed. In this case, the slave moves toward the position of the master that has to be kept still by the user. In [28], a controller for improving position tracking in bilateral teleoperation via packet-switched networks is developed, while in [29], a method to reduce the position drift without violating system passivity conditions is proposed. It is worth highlighting that the mentioned approaches do not consider autonomous modes and, therefore, always produce a bilateral action, moving both master and slave.

III. Background on Port-Hamiltonian Systems and Energy Tanks

This section provides some background on port-Hamiltonian systems and on energy tanks. For a more detailed treatment, see [8], [10], and [30].

The port-Hamiltonian framework is a generalization of standard Hamiltonian mechanics, where energetic characteristics and power exchange between subsystems are clearly identified. All physical systems, even multidomain, can be represented using the port-Hamiltonian formalism. The most common representation of a port-Hamiltonian system is

$$\begin{cases} \dot{x} = [J(x) - R(x)] \dfrac{\partial H}{\partial x} + g(x)u \\ y = g^T(x) \dfrac{\partial H}{\partial x} \end{cases} \tag{1}$$

where $x \in \mathbb{R}^n$ is the state vector, and $H(x) : \mathbb{R}^n \to \mathbb{R}$ is the lower bounded Hamiltonian function representing the amount of energy stored in the system. Matrices $J(x) = -J(x)^T$ and $R(x) \geq 0$ represent the internal energetic interconnections and the dissipation of the port-Hamiltonian system, respectively, and $g(x)$ is the input matrix. The input u and the output y are dual variables and their product is (generalized) power. The pair (u, y) is called power port and is the means by which the system can energetically interact with the external world. The product $u^T y$ represents the power exchanged by the system with the external world.

It can be easily shown that the following equality holds [8]:

$$\dot{H}(x) + \frac{\partial^T H}{\partial x} R(x) \frac{\partial H}{\partial x} = u^T(t) y(t). \tag{2}$$

This means that the power supplied to the system is either stored or dissipated, namely that a port-Hamiltonian system is passive with respect to the pair (u, y). Let

$$D(x) = \frac{\partial^T H}{\partial x} R(x) \frac{\partial H}{\partial x} \geq 0 \tag{3}$$

indicate the power dissipated by the system. As pointed out in [31], $D(x)$ represents a *passivity margin*: the larger $D(x)$, higher the passivity of the system. In other words, the larger the passivity margin, the more the system can absorb the energy generated by nonpassive actions (e.g., changing the stiffness in a viscoelastic coupling, as discussed later) while preserving its passivity.

Energy tanks, first proposed in [9], exploit this concept for building flexible and passivity preserving controllers. The energy dissipated by the system is stored in a (virtual) energy tank and can be reused for implementing any desired control action in a passivity preserving way.

More formally, the dynamics of a port-Hamiltonian system endowed with a tank is given by

$$\begin{cases} \dot{x} = [J(x) - R(x)] \dfrac{\partial H}{\partial x} + g(x)u \\ \dot{x}_t = \dfrac{\sigma}{x_t} D(x) + \dfrac{1}{x_t} (\sigma P_{\text{in}} - P_{\text{out}}) + u_t \\ y_1 = \begin{pmatrix} y \\ y_t \end{pmatrix} \end{cases} \tag{4}$$

where $x_t \in \mathbb{R}$ is the state associated with the energy storing tank, and

$$T(x_t) = \frac{1}{2} x_t^2 \tag{5}$$

is the energy stored in the tank. $P_{\text{in}} \geq 0$ and $P_{\text{out}} \geq 0$ are incoming and outgoing power flows that the tank can exchange with other tanks, respectively. The pair (u_t, y_t) is a power port that the tank can use to exchange energy with the external world and $y_t = \frac{\partial T}{\partial x_t} = x_t$. The parameter $\sigma \in \{0, 1\}$ is used for bounding the amount of energy that can be stored in the tank. The following power balance can be easily derived from (4):

$$\dot{T} = \sigma D(x) + \sigma P_{\text{in}} - P_{\text{out}} + u_t^T y_t \tag{6}$$

which means that, if $\sigma = 1$, the tank stores the power dissipated by the system $D(x)$ and the incoming power flow P_{in}, while

the outgoing power flow P_{out} is released. Furthermore, energy can be injected in / extracted from the tank via the power port (u_t, y_t). In order to avoid singularities in (4), some energy must always be present in the tank (i.e., $x_t \neq 0$). Thus, it is necessary to set an arbitrarily small threshold $\varepsilon > 0$ representing the minimum amount of energy that needs to be always stored. The tank has to be initialized and managed in such a way that $T(x_t(0)) > \varepsilon$ and energy extraction is prevented if $T(x_t) \leq \varepsilon$. Finally, it is necessary to set an upper bound on the amount of energy that can be stored in the tank. In fact, as described in [32], if there is no bound, the energy available can become very large as time increases, and even if the system remains passive, it would be possible to implement behaviors that are unstable in practice. Thus, σ is set using the following policy:

$$\sigma = \begin{cases} 1, & \text{if } T(x_t) \leq \bar{T} \\ 0, & \text{otherwise} \end{cases} \tag{7}$$

where $\bar{T} > 0$ is a suitable application-dependent upper bound on the energy that can be stored in the tank.

The energy stored in the tank can be exploited for passively implementing any desired input $w \in \mathbb{R}^n$ to the port-Hamiltonian system the tank is associated with. This can be done by joining the power ports (u, y) and (u_t, y_t) through the following power preserving interconnection:

$$\begin{cases} u = \dfrac{w}{x_t} y_t = \dfrac{w}{x_t} x_t = w \\ u_t = -\dfrac{w^T}{x_t} y \end{cases} \tag{8}$$

implying the balance

$$u^T y = -u_t y_t. \tag{9}$$

When using (8) the energy supplied to/extracted from the port-Hamiltonian system for implementing the desired input is exactly equal to the energy extracted from/supplied to the tank. This intuitively means that no energy is generated and that the desired input can be implemented in a way to preserve passivity as long as some energy is stored in the tank (i.e. $T(x_t) > \varepsilon$). For a more formal treatment, see [10] and [30].

IV. Variable Admittance Control

Admittance control and impedance control [33] are very effective control schemes for implementing a desired interaction behavior. Loosely speaking, impedance control is more suitable for backdrivable robots, while admittance control is more suitable for stiff robots. The robot developed within the I-SUR project has a stiff and not backdrivable structure. Therefore, we will show how to exploit tanks for implementing a variable admittance control. However, all the results developed in this section can be easily adapted for implementing a variable impedance control (see, e.g., [11] for a variable stiffness impedance controller).

A standard admittance control scheme is reported in Fig. 1. Given a desired interaction model, namely a dynamic relation between the applied force and the pose error, given the external

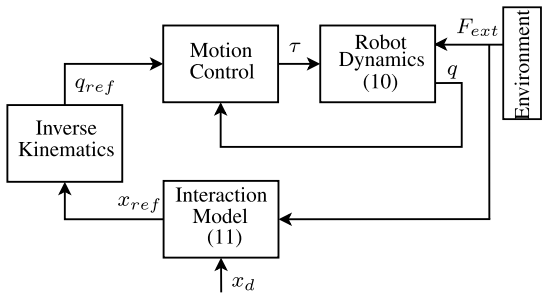

Fig. 1. Control scheme for admittance control with underlying motion controller. The solution of the interaction model (11) with the inputs F_{ext} and x_d provides the value x_{ref} which the position-controlled robot must follow.

force and the desired pose setpoint, the corresponding position of the robot is generated and tracked by the robot by means of a lower level motion controller. We expect the latter to be designed and tuned to minimize the tracking error and optimize the dynamic response so that we can assume that the actual pose $x \in \mathbb{R}^n$, $n \leq 6$, of the robot end-effector is identical to its reference position x_{ref}. Thus, in the following, we will consider $x = x_{\text{ref}}$.

More formally, consider the following Euler–Lagrange dynamic model of a fully actuated n-degree-of-freedom (DOF) manipulator in the task space:

$$\Lambda(x)\ddot{x} + \mu(x, \dot{x})\,\dot{x} + F_g(x) = F_\tau + F_{\text{ext}} \tag{10}$$

where $x = f(q)$ is the pose of the end-effector, obtained from the joint positions $q \in \mathbb{R}^m$, $m \geq n$, through the forward kinematic map $f(\cdot)$, $F_{\text{ext}} \in \mathbb{R}^n$ is the external wrench applied to the end-effector, and $F_\tau \in \mathbb{R}^n$ is the wrench due to the controlled joint torques $\tau \in \mathbb{R}^m$. $\Lambda(x) = \Lambda^T(x) > 0$ is the n-dimensional positive-definite inertia matrix, $\mu(x, \dot{x}) \in \mathbb{R}^{n \times n}$ is the matrix of the centrifugal and Coriolis terms, and $F_g(x) \in \mathbb{R}^n$ is the wrench due to the gravity. The control wrench F_τ is set by the motion controller for implementing a desired interactive behavior.

A very common interaction model adopted in standard admittance control is the multidimensional mass–spring–damper system described by

$$\Lambda_d \ddot{\tilde{x}} + D_d \dot{\tilde{x}} + K_d \tilde{x} = F_{\text{ext}} \tag{11}$$

where $\tilde{x}(t) = x(t) - x_d(t)$ is the pose error. Λ_d, D_d, and K_d are the n-dimensional symmetric and positive-definite inertia, damping, and stiffness matrices characterizing the interactive behavior. The controlled robot behaves as (11), and it is passive with respect to the pair $(F_{\text{ext}}, \tilde{x})$. In fact, consider

$$V(\tilde{x}, \dot{\tilde{x}}) = \frac{1}{2} \dot{\tilde{x}}^T \Lambda_d \dot{\tilde{x}} + \frac{1}{2} \tilde{x}^T K_d \tilde{x} \tag{12}$$

as a nonnegative storage function. We have that

$$\dot{V} = \dot{\tilde{x}}^T \Lambda_d \ddot{\tilde{x}} + \tilde{x}^T K_d \dot{\tilde{x}}. \tag{13}$$

Using (11) in (13), we obtain

$$\dot{V} = \dot{\tilde{x}}^T F_{\text{ext}} - \dot{\tilde{x}}^T D_d \dot{\tilde{x}} \leq \dot{\tilde{x}}^T F_{\text{ext}} \tag{14}$$

which implies the passivity condition

$$V(t) - V(0) \leq \int_0^t \dot{\tilde{x}}^T(\tau) F_{\text{ext}}(\tau) d\tau. \tag{15}$$

The passivity of the controlled behavior is a crucial characteristic of admittance control. In fact, passivity is a sufficient condition for ensuring a stability of the controlled robot both in free motion and during the interaction with any passive, possibly unknown, environment [8]. Furthermore, in case of free motion (i.e., $F_{\text{ext}} = 0$), using (12) as a Lyapunov function and considering (14), it can be shown by a straightforward application of LaSalle's invariance principle that $\tilde{x}(t) \mapsto 0$, i.e., that the robot asymptotically tracks the desired reference.

A. Problem Formulation

Our goal is to develop a variable admittance control that allows the robot to reproduce the behavior of the surgeon during operations [34] and that is as unconstrained as possible in order to provide high flexibility to the interactive robot.

Let $\Lambda_d(t)$, $D_d(t)$, and $K_d(t)$ be the time-varying inertia, damping, and stiffness matrices. The desired interaction model is given by

$$\Lambda_d(t)\ddot{\tilde{x}} + D_d(t)\dot{\tilde{x}} + K_d(t)\tilde{x} = F_{\text{ext}}. \tag{16}$$

In order to preserve their physical meaning, we assume that $\Lambda_d(t)$, $D_d(t)$, and $K_d(t)$ are symmetric and positive definite for all $t \geq 0$.

The main drawback due to the introduction of a variable interaction model in an admittance control scheme is the loss of passivity of the controlled robot. In fact, consider the total energy of the controlled system as a natural nonnegative storage function:

$$\mathcal{V}(\tilde{x}, \dot{\tilde{x}}) = \frac{1}{2}\dot{\tilde{x}}^T \Lambda_d(t)\dot{\tilde{x}} + \frac{1}{2}\tilde{x}^T K_d(t)\tilde{x}. \tag{17}$$

We have that

$$\dot{\mathcal{V}} = \dot{\tilde{x}}^T \Lambda_d(t)\ddot{\tilde{x}} + \frac{1}{2}\dot{\tilde{x}}^T \dot{\Lambda}_d(t)\dot{\tilde{x}} + \tilde{x}^T K_d(t)\dot{\tilde{x}} + \frac{1}{2}\tilde{x}^T \dot{K}_d(t)\tilde{x}. \tag{18}$$

Computing $\ddot{\tilde{x}}$ from (16) and replacing it in (18), we obtain

$$\dot{\mathcal{V}} = \dot{\tilde{x}}^T F_{\text{ext}} + \left[\frac{1}{2}\dot{\tilde{x}}^T(\dot{\Lambda}_d(t) - 2D_d(t))\dot{\tilde{x}} + \frac{1}{2}\tilde{x}^T \dot{K}_d(t)\tilde{x}\right]. \tag{19}$$

Because of the variability of the stiffness and of the inertia, the term between the brackets can be positive and the system can produce energy, and therefore, the balance in (15) is not always satisfied. Consequently, the passivity of the interaction model does not hold anymore and a stable interaction and an asymptotic tracking in free motion are no longer guaranteed.

In the rest of the section, we will show how it is possible, using energy tanks, to implement the flexible interaction model (16) while preserving the passivity of the controlled robot.

B. Variable Admittance

The main idea for implementing a variable admittance controller is to endow the desired interaction model with a tank for storing the energy dissipated by the system and for reusing it for implementing passivity threatening variable behaviors in a passive way.

We split the variable inertia and stiffness matrices into the sum of a constant term and of a variable term:

$$\begin{cases} \Lambda_d(t) = \Lambda_c + \Lambda_v(t) \\ K_d(t) = K_c + K_v(t) \end{cases} \tag{20}$$

where Λ_c, K_c, $\Lambda_v(t)$, and $K_v(t)$ are symmetric positive-definite matrices. The constant terms may represent the minimum implementable inertia and stiffness, but, in general, it is sufficient for them to be constant, symmetric, and positive definite, and they can represent other significant values. The variable terms can be designed using profiles arbitrarily chosen, even discontinuous.

Considering (20), it is possible to reformulate the interaction model (16) as a port-Hamiltonian system as

$$\begin{cases} \begin{pmatrix} \dot{\tilde{x}} \\ \dot{\tilde{p}} \end{pmatrix} = \begin{pmatrix} 0 & I \\ -I & -K_d(t) \end{pmatrix} \begin{pmatrix} \dfrac{\partial H_c}{\partial \tilde{x}} \\ \dfrac{\partial H_c}{\partial \tilde{p}} \end{pmatrix} + \begin{pmatrix} 0 \\ I \end{pmatrix} F_{\text{ext}} + \\ \qquad\qquad + \begin{pmatrix} 0 \\ I \end{pmatrix} (-K_v(t)\tilde{x} - \Lambda_v(t)\ddot{\tilde{x}}) \\ y = \dot{\tilde{x}} \end{cases} \tag{21}$$

where $\tilde{p} = \Lambda_c \dot{\tilde{x}}$ and

$$H_c(\tilde{x}, \tilde{p}) = \frac{1}{2}\tilde{x}^T K_c \tilde{x} + \frac{1}{2}\tilde{p}^T \Lambda_c^{-1} \tilde{p}. \tag{22}$$

As is evident in (21), the variability of the inertia and of the stiffness matrix produce an extra input in the port-Hamiltonian dynamics, and this input can inject energy into the system destroying its passivity. In order to overcome this problem, we augment the port-Hamiltonian interaction model with a tank. In this manner, we keep trace of the dissipated energy, and we can exploit it for passively implementing the extra input due to the variability of the admittance parameters. Thus, we propose the following augmented port-Hamiltonian interaction model:

$$\begin{cases} \begin{pmatrix} \dot{\tilde{x}} \\ \dot{\tilde{p}} \end{pmatrix} = \begin{pmatrix} 0 & I \\ -I & -K_d(t) \end{pmatrix} \begin{pmatrix} \dfrac{\partial H_c}{\partial \tilde{x}} \\ \dfrac{\partial H_c}{\partial \tilde{p}} \end{pmatrix} + \begin{pmatrix} 0 \\ I \end{pmatrix} F_{\text{ext}} + \begin{pmatrix} 0 \\ I \end{pmatrix} w \\ \dot{x}_t = \dfrac{\sigma}{x_t} \tilde{p}^T \Lambda_c^{-1} K_d(t) \Lambda_c^{-1} \tilde{p} - \dfrac{w^T}{x_t} \dot{\tilde{x}} \\ y = \dot{\tilde{x}} \end{cases} \tag{23}$$

where $x_t \in \mathbb{R}$ and $T(x_t) = \frac{1}{2}x_t^2$ are the state and the energy function of the tank, respectively. The parameter $\sigma \in \{0, 1\}$ is used to disable the dissipated energy storage in case a maximum limit is reached. The tank initial state is set to $x_t(0)$ such that $T(x_t(0)) > \varepsilon$ and

$$w(t) = \begin{cases} (-K_v(t)\tilde{x} - \Lambda_v(t)\ddot{\tilde{x}}), & \text{if } T(x_t) > \varepsilon \\ 0, & \text{otherwise.} \end{cases} \tag{24}$$

The energy stored in the tank is exploited for implementing the input due to the variability of the stiffness and inertia parameters. If there is some energy stored in the tank, the desired interaction model is implemented; otherwise, the variable parts of the admittance parameters are not implemented. This means that the priority is always given to passivity: If the variable interaction model cannot be implemented using the available energy, then a passive constant behavior, associated with the constant parameters Λ_c and K_c, is implemented.

The power extracted from the tank for implementing the desired behavior is given by

$$u_t y_t = \frac{w^T}{x_t}\dot{\tilde{x}}x_t = -\tilde{x}^T K_v(t)\dot{\tilde{x}} - \ddot{\tilde{x}}^T \Lambda_v(t)\dot{\tilde{x}}. \tag{25}$$

Thus, if the variability of the inertia and of the stiffness with respect to Λ_c and K_c is small and/or if the tracking error is small, the energy necessary for implementing the desired behavior is small, and therefore, it is very likely that the energy stored in the tank is sufficient for passively reproducing the desired behavior. Furthermore, it is possible to temporarily increase the value of the desired damping for storing more energy into the tank and increasing the flexibility of the system at the price of a (temporarily) overdamped behavior.

Remark 1: In order to shape both the inertia and the stiffness matrices, an acceleration measurement (or estimation) is necessary. If this is not available, the desired inertia should remain constant, but it would still be possible to shape the stiffness matrix using only position measurements.

Proposition 1: The augmented port-Hamiltonian interaction model (23) is passive with respect to the pair $(F_{\text{ext}}, \dot{\tilde{x}})$.

Proof: Consider as a storage function the total energy of the system

$$W(t) = H_c(\tilde{x}, \tilde{p}) + T(x_t) = \frac{1}{2}\tilde{x}^T K_c \tilde{x} + \frac{1}{2}\tilde{p}^T \Lambda_c^{-1}\tilde{p} + \frac{1}{2}x_t^2. \tag{26}$$

The interaction model in (23) can be rewritten as

$$\begin{cases} \begin{pmatrix} \dot{\tilde{x}} \\ \dot{\tilde{p}} \\ \dot{x}_t \end{pmatrix} = \left[\begin{pmatrix} 0 & I & 0 \\ -I & 0 & \frac{w}{x_t} \\ -\frac{w^T}{x_t} & 0 & 0 \end{pmatrix} - \right. \\ \left. \begin{pmatrix} 0 & 0 & 0 \\ 0 & K_d(t) & 0 \\ -P(t) & 0 & 0 \end{pmatrix} \right] \begin{pmatrix} \frac{\partial W}{\partial \tilde{x}} \\ \frac{\partial W}{\partial \tilde{p}} \\ \frac{\partial W}{\partial x_t} \end{pmatrix} + \begin{pmatrix} 0 \\ I \\ 0 \end{pmatrix} F_{\text{ext}} \\ y = \dot{\tilde{x}} \end{cases} \tag{27}$$

where $P(t) = \frac{\sigma}{x_t}\tilde{p}^T \Lambda_c^{-1} K_d(t)$. Considering (27), from simple computations, it follows that

$$\begin{aligned} \dot{W} =& -\tilde{p}^T \Lambda_c^{-1} K_d(t) \Lambda_c^{-1}\tilde{p} + \sigma \tilde{p}^T \Lambda_c^{-1} K_d(t) \Lambda_c^{-1}\tilde{p} + F_{\text{ext}}^T \dot{\tilde{x}} = \\ =& -\tilde{p}^T \Lambda_c^{-1}(K_d(t) - \sigma K_d(t))\Lambda_c^{-1}\tilde{p} + F_{\text{ext}}^T \dot{\tilde{x}}. \end{aligned} \tag{28}$$

Since $\sigma \in \{0, 1\}$ and since $K_d(t) > 0$, then $(K_d(t) - \sigma K_d(t)) \geq 0$, and therefore, $\dot{W} \leq F_{\text{ext}}^T \dot{\tilde{x}}$ which implies

$$W(t) - W(0) \leq \int_0^t F_{\text{ext}}^T \dot{\tilde{x}} d\tau \tag{29}$$

which proves passivity. ■

Thanks to the energy tank, it is possible to implement any variable interaction model satisfying the passivity constraint that guarantees a stable behavior and asymptotic tracking in free motion. For further details and additional experiments showing the instability of the system when using standard impedance controllers with variable stiffnesses, see [11].

V. Switching From Autonomous to Teleoperated Mode

A. Problem Formulation

The problem of switching from autonomous to teleoperated mode in a stable way will be addressed using energetic considerations, and therefore, it is convenient to formulate the problem in the port-Hamiltonian framework.

When switching from the autonomous mode to the teleoperated mode, there is a fully actuated surgical robot, the slave, that has to be teleoperated by means of a fully actuated mechanical interface, the master. In the following formulation, we will consider bilateral teleoperation, where the teleoperated robot reflects back to the master reaction forces from the task being performed.

Master and slave robots can be modeled as port-Hamiltonian systems as

$$\begin{cases} \begin{pmatrix} \dot{x}_i \\ \dot{p}_i \end{pmatrix} = \begin{pmatrix} 0 & I \\ -I & -R_i \end{pmatrix} \begin{pmatrix} \frac{\partial H_i}{\partial x_i} \\ \frac{\partial H_i}{\partial p_i} \end{pmatrix} + \begin{pmatrix} 0 \\ I \end{pmatrix} F_{\text{ext},i} + \begin{pmatrix} 0 \\ I \end{pmatrix} F_i \\ y_i = \begin{pmatrix} 0 & I \end{pmatrix} \begin{pmatrix} \frac{\partial H_i}{\partial x_i} \\ \frac{\partial H_i}{\partial p_i} \end{pmatrix} = v_i \qquad i = m, s \end{cases} \tag{30}$$

where $x_i \in \mathbb{R}^n$, $p_i \in \mathbb{R}^n$, and $v_i \in \mathbb{R}^n$ represent the pose, the momentum, and the velocity, respectively. H_i is the kinetic energy of the robot, and R_i is a symmetric positive-definite matrix representing the damping in the system, possibly augmented using local damping injection [8]. F_i is the generalized force due to the bilateral coupling, while $F_{\text{ext},i}$ represents the force due to the interaction with the external world. For the master and the slave, this force is indicated by F_h, the force applied by the human, and by F_e, the force applied by the environment, respectively. We consider the situation where the surgeon is in the proximity of the surgical robot, and therefore, we assume a negligible communication delay between the master and the slave. Because of their robustness, indirect force feedback teleoperation systems have proven to be very effective in several applications, and therefore, we will consider this kind of coupling between master and slave. Several control strategies are available in the literature, but one of the most simple, efficient, and commonly used is a PD coupling (see, e.g., [35], [36]) that

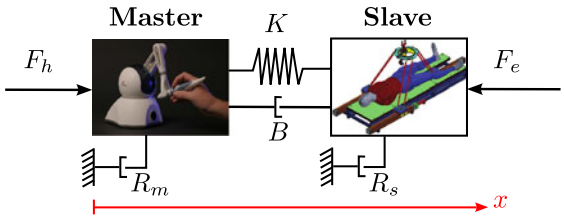

Fig. 2. Master and slave are interconnected with a virtual spring–damper system equivalent to a PD coupling.

is described by

$$\begin{cases} F_m = -K(x_m - x_s) - B(\dot{x}_m - \dot{x}_s) \\ F_s = +K(x_m - x_s) + B(\dot{x}_m - \dot{x}_s) \end{cases} \tag{31}$$

where $K \in \mathbb{R}^{n\times n} > 0$ and $B \in \mathbb{R}^{n\times n} > 0$ are the proportional and the derivative gains, respectively. This is equivalent to interconnect master and slave with a (virtual) spring–damper system as illustrated in Fig. 2. Since the PD controller is a passive system, and master and slave are passive port-Hamiltonian systems, the overall teleoperation system is passive, and therefore, it is characterized by a stable behavior. Furthermore, in case master and slave are initially aligned, a PD coupling guarantees a steady-state position tracking and, in case of interaction with the environment, a perfect steady-state force tracking [8].

Nevertheless, in case of an initial position mismatch, a PD coupling may be problematic. In fact, suppose that at time t_s, the surgical system switches from autonomous to teleoperated mode. If master and slave robots are immobile but misaligned, an abrupt force $K(x_m(t_s) - x_s(t_s))$ is applied, with different sign, to both robots. At the master side, this force provides an abrupt and, possibly, unexpected feedback to the user, while at the slave side, it generates a motion that may even be unacceptable, as is the case when the surgical tool is close to an organ. This abrupt force makes the control strategy (31) too dangerous to be used in surgical applications.

A simple but not too effective solution to this problem consists of two steps. First, the pose of the master is taken to the same (scaled) pose of the slave, and second, the teleoperation system is started. The main advantage of this strategy is that master and slave positions match, and using standard teleoperation strategy, a zero steady-state position error can be achieved. The main drawback of this approach is the waiting time necessary for the alignment of the master. This waiting time cannot always be tolerable, especially in emergency situations. Furthermore, since positioning is made by standard PID controllers and an integral action on the position is needed for compensating the gravity effect, if the surgeon by accident (e.g., because of the rush due to the emergency) grasps and moves the master before the alignment is over, an unstable behavior may arise [8] and the waiting time for activating the teleoperation system may increase.

In order to preserve the passivity of the overall teleoperation system and to get rid of abrupt forces due to the robots initial misalignment, we propose to modify (31) as

$$\begin{cases} F_m = -K(x_m - x_s - L) - B(\dot{x}_m - \dot{x}_s) \\ F_s = +K(x_m - x_s - L) + B(\dot{x}_m - \dot{x}_s) \end{cases} \tag{32}$$

where $L = x_m(t_s) - x_s(t_s)$ is the pose offset when the teleoperated mode is switched ON. This way, the coupling force transmitted to the robots is zero. Furthermore, (32) is still physically equivalent to a spring–damper system, where the spring has a rest length L. It can be easily shown that this controller is passive and that, consequently, the overall teleoperation system is passive being the interconnection of passive systems. Thus, using the controller (32), when the teleoperated mode is switched ON, the surgeon can start using the system without waiting time, and the system does not transmit any abrupt force during the switch ON. However, also this approach is not fully satisfactory because the surgeon has to mentally compensate for the position offset all the time, and this may prevent her/him to focus on the primary task, namely emergency handling. Furthermore, the force/torque feedback received from the slave side is misleading due to the pose mismatch.

In the next section, we will show how to exploit (32) for removing abrupt switching forces and how to design a passivity preserving control strategy generating a compensating force that reduces the waiting time with respect to the simplistic solution described above.

B. Two-Layer Architecture for Compensating the Pose Offset

The steady-state position error obtained when using (32) is due to the fact that the spring-like term of the controller has a nonzero rest length L that, nevertheless, is necessary for preventing an abrupt force when the teleoperated mode is switched ON.

The main idea for compensating the pose offset while avoiding abrupt initial forces is to gradually decrease the value of the rest length toward zero. In other words, the constant rest length L of (32) will be replaced by a continuous time function $l(t)$ such that $l(t_s) = L$ and $l(t) = 0$ for $t \geq t_s + t_c$. The time evolution of $l(t)$ and the amount of time $t_c - t_s$ necessary for completing the compensation are free parameters that can be set by the designer.

Nevertheless, since (32) is a bilateral interconnection, when the rest length of the spring-like element is changing, an elastic force is applied both to the master and to the slave. This effect is undesired because the force due to the compensation will cause a motion of the slave that is not directly commanded by the surgeon and this is unacceptable since injury may be caused to the patient.

Thus, we propose to implement the following coupling between master and slave:

$$\begin{cases} F_{md} = -K(x_m - x_s - l(t)) - B(\dot{x}_m - \dot{x}_s) \\ F_{sd} = \alpha(t)[K(x_m - x_s - l(t)) + B(\dot{x}_m - \dot{x}_s)] \end{cases} \tag{33}$$

where F_{md} and F_{sd} indicate the desired values of F_m and F_s, respectively. The smooth function $\alpha(t) : \mathbb{R} \mapsto [0, 1]$ is used for

weighting the desired force to be applied to the slave side, and it is defined by

$$\alpha(t) = \begin{cases} \alpha_1(t)\alpha_2(t), & \text{if } t_s < t < t_M \\ 1, & \text{if } t \geq t_M \end{cases} \tag{34}$$

where t_M is the first instant of time at which $\alpha_1(t)\alpha_2(t) = 1$. Loosely speaking, when $\alpha(t)$ reaches its maximum value, it holds it. Let $e(t) = \|x_m(t) - x_s(t)\|$ be the norm of the position error, and let $\lambda(t) = \|l(t)\|$. The map $\alpha_1 = \alpha_1(e(t)) : \mathbb{R}^+ \mapsto [0, 1]$ is a smooth real function defined as

$$\alpha_1(e(t)) = \begin{cases} 1, & \text{if } e(t) \leq \bar{e}_1 \\ f_1(e(t)), & \text{if } \bar{e}_1 < e(t) < \bar{e}_2 \\ 0, & \text{if } e(t) \geq \bar{e}_2 \end{cases} \tag{35}$$

where $f_1(e(t))$ is a nonincreasing function, and $\bar{e}_1 < \bar{e}_2$ are thresholds that can be set by the designer. Similarly, $\alpha_2 = \alpha_2(\lambda(t)) : \mathbb{R}^+ \mapsto [0, 1]$ is a smooth real function defined as

$$\alpha_2(\lambda(t)) = \begin{cases} 1, & \text{if } \lambda(t) \leq \bar{\lambda}_1 \\ f_2(\lambda(t)), & \text{if } \bar{\lambda}_1 < \lambda(t) < \bar{\lambda}_2 \\ 0, & \text{if } \lambda(t) \geq \bar{\lambda}_2 \end{cases} \tag{36}$$

where $f_2(\lambda(t))$ is a nonincreasing function, and $\bar{\lambda}_1 < \bar{\lambda}_2$ are thresholds that can be set by the designer. Functions α_1 and α_2 are used to weight the position error and the rest length. Only when both $e(t)$ and $\lambda(t)$ are small enough, $\alpha(t) = 1$ and (33) is equivalent to (31). This way, a standard bilateral interconnection between master and slave will be established only when the position offset is close to zero (i.e., no compensating effort requested to the user) and when the position error is close to zero (i.e., no abrupt switching force). By properly choosing the thresholds in (35) and (36), it is possible to tune the interconnection phase. Possible guidelines for setting the thresholds are given by the following considerations. Greater values of $\bar{e}_2$ and $\bar{\lambda}_2$ will delay the moment when the slave starts to feel the reflected force, while greater values of $\bar{e}_1$ and $\bar{\lambda}_1$ will lead to an earlier enabling of the completely bilateral interconnection (i.e., α reaches 1 with a larger offset and a larger position error). The difference between $\bar{e}_2$ and $\bar{e}_1$ ($\bar{\lambda}_2$ and $\bar{\lambda}_1$) specifies the duration of the transient phase. In the transient phase, when $0 < \alpha_1 < 1$ or $0 < \alpha_2 < 1$, the control force applied to the slave is scaled by the gain $\alpha(t)$ that is as small as the situation is difficult for the surgeon to control (i.e., big position error and big rest length). As long as $\alpha(t) = 0$, instead, the slave is disconnected from the bilateral controller, and no force is applied to the surgical robot. At the master side, the surgeon receives a force feedback due to the compensation. The feedback attracts the surgeon toward a pose of the master that is aligned with that of the slave, acting like a sort of virtual fixture. This makes the compensation process faster than a simple position controller since the user drives the master toward the desired pose, and this action is superimposed to the one of the coupling controller.

Thus, using (33), the switching between automatic and teleoperated mode is smooth, a virtual fixture attracts the surgeon toward an aligned pose, and the compensation process does not cause undesired motions of the slave robot. Nevertheless, it is well known that changing the rest length of a spring is not a passivity preserving operation (see, e.g., [8]). Furthermore, unlike (32), the coupling reported in (33) is asymmetric, and this asymmetry destroys the passivity of the controller. This loss of passivity makes the teleoperation system potentially unstable and unsafe to use.

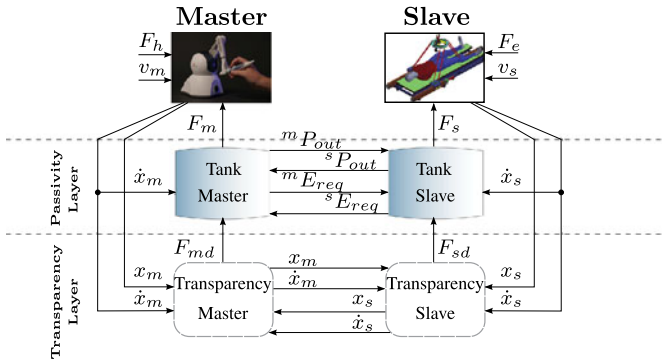

Fig. 3. Two-layer architecture for the pose offset compensation. In the *Transparency Layer*, the desired coupling forces are computed according to (33). These commands are sent to the *Passivity Layer*, whose role is to check and guarantee the passivity of the total system.

In order to recover the passivity of the teleoperation system and to preserve the performance of (33), we propose to exploit the two-layer framework proposed in [10]. The overall architecture is reported in Fig. 3, and it can be decomposed into two layers: a *Transparency Layer* and a *Passivity Layer*.

First of all, master and slave robots are augmented with a tank, as described in Section III, in order to have a storage of energy that can be used for implementing external desired control actions.

In the Transparency Layer, master and slave exchange position and velocity information that is used for computing the desired coupling forces, namely F_{md} and F_{sd} defined in (33). These forces are sent to the Passivity Layer whose role is to passively implement them using the energy stored in the tanks. Master and slave energy tanks can exchange power for balancing the amount of energy stored at master and slave side. Formally, the augmented master and slave sides are modeled as

$$\begin{cases} \begin{pmatrix} \dot{x}_i \\ \dot{p}_i \end{pmatrix} = \begin{pmatrix} 0 & I \\ -I & -R_i \end{pmatrix} \begin{pmatrix} \dfrac{\partial H_i}{\partial x_i} \\ \dfrac{\partial H_i}{\partial p_i} \end{pmatrix} + \begin{pmatrix} 0 \\ I \end{pmatrix} F_{ext,i} + \begin{pmatrix} 0 \\ I \end{pmatrix} F_i \\ \dot{x}_{t_i} = \dfrac{\sigma_i}{x_{t_i}} D_i(x_i) + \dfrac{1}{x_{t_i}} (\sigma_i {}^iP_{\text{in}} - {}^iP_{\text{out}}) + u_{t_i} \\ y_i = \begin{pmatrix} v_i \\ y_{t_i} \end{pmatrix} \qquad i = m, s \end{cases} \tag{37}$$

where x_{t_i}, $y_{t_i} = x_{t_i}$, and $T_i = \frac{1}{2} x_{t_i}^2$ are the state of the tank, the output associated to the tank, and the energy stored in the tank, respectively. D_i is the energy dissipated by the robot (that can be augmented by introducing a local damping injection [30]), and ${}^iP_{\text{in}}$ and ${}^iP_{\text{out}}$ are the power flows that can be exchanged with the other tank.

The desired coupling forces are implemented using the energy stored in the tanks by interconnecting the power port of the tank (u_{t_i}, y_{t_i}) with the power port of the robot (F_i, v_i) using the following power preserving interconnection:

$$\begin{cases} F_i = \dfrac{F_{id}}{x_{t_i}} y_{t_i} = \dfrac{F_{id}}{x_{t_i}} x_{t_i} = F_{id} \\ \\ u_{t_i} = -\dfrac{F_{id}^T}{x_{t_i}} v_i \end{cases} \qquad i = m, s. \tag{38}$$

As shown in (8) and (9), (38) is a power preserving interconnection, and therefore, the desired input F_{id} is implemented by exchanging energy with the tank: If $F_{id}^T v_i > 0$, it means that some energy is necessary for implementing the desired input, and consequently, this energy is extracted from the tank. On the other hand, if $F_{id}^T v_i < 0$, it means that the desired action is dissipative, and therefore, the dissipated energy is stored in the tank.

The desired coupling forces can be passively achieved if and only if tanks are full enough. As reported in Section III, if the energy of the tank T_i goes below a predefined threshold ε_i, energy extraction is forbidden and the coupling force implemented is $F_i = 0$. This guarantees passivity and, therefore, a stable behavior of the teleoperation system, but negatively affects performance. Thus, it is necessary to ensure that, at both master and slave side, the fill level of the tank is kept much higher than the minimum. The energy stored in the tanks can be augmented in two ways: receiving energy from the other tank or augmenting the damping of the associated robot by means of damping injection. The latter option should be used as a last resort since it is an invasive option, and the extra damping will be felt by the user and/or will modify the dynamics of the slave changing the desired coupling (33).

An exchange of energy between master's and slave's tanks affects only the amount of energy available for implementing a desired control action, and it does not have any direct effect on the dynamics of the teleoperation system. Following the approach suggested in [37], we implement the following exchange strategy: When the energy of the tank of the master goes below a desired threshold ${}^m T_{\rm req}$, an energy request ${}^m E_{\rm req}$ is sent to the slave tank. If the amount of energy available in the tank of the slave is greater than a threshold ${}^s T_{\rm ava}$, a flow of energy is sent to the master tank. Furthermore, the slave tank sends to the master tank also the energy dissipated by the robot that cannot be stored in the tank because it reached its upper threshold $\bar{T}_s$. An analogous behavior is implemented at the slave side. Formally, we have that the energy request signal is given by

$${}^i E_{\rm req} = \begin{cases} 1, & \text{if } T_i(x_{t_i}) < {}^i T_{\rm req} \\ 0, & \text{otherwise} \end{cases} \qquad i = m, s. \tag{39}$$

The overall power extracted from each tank and sent to the other tank is then given by

$$\begin{cases} {}^m P_{\rm out} = (1-\sigma_m) D_m + {}^s E_{\rm req} \beta_m \bar{P} = {}^s P_{\rm in} \\ \\ {}^s P_{\rm out} = (1-\sigma_s) D_s + {}^m E_{\rm req} \beta_s \bar{P} = {}^m P_{\rm in} \end{cases} \tag{40}$$

where the energy dissipated by the robot is sent to the other tank if and only if the tank is already full (i.e., $\sigma_i = 1$). The variable $\beta_i \in \{0, 1\}$ disables/enables the transfer of the energy stored in the tank, and it is given by

$$\beta_i = \begin{cases} 1, & \text{if } T_i(x_{t_i}) \geq {}^i T_{\rm ava} \\ 0, & \text{otherwise} \end{cases} \qquad i = m, s. \tag{41}$$

The variable $\bar{P} > 0$ is the rate of energy flowing from one tank to the other, and it is a design parameter. The bigger is $\bar{P}$, the faster is the energy transfer. All the thresholds mentioned so far are also design parameters, and the following constraints must be satisfied: $\varepsilon_i < {}^i T_{\rm req} < {}^i T_{\rm ava} < \bar{T}_i$, for $i = m, s$.

The strategy illustrated so far guarantees the passivity of the teleoperation system as proven in the following.

Proposition 2: The overall teleoperation system is passive with respect to the pair $((F_h^T, F_e^T)^T, (v_m^T, v_s^T)^T)$.

Proof: Consider the total energy of the teleoperation system as a storage function:

$$\mathcal{H}(t) = H_m(t) + H_s(t) + T_m(t) + T_s(t). \tag{42}$$

Using (37), we obtain that

$$\begin{aligned} \dot{\mathcal{H}}(t) = & -D_m(t) - D_s(t) + F_m^T v_m + F_s^T v_s + \\ & + \sigma_m D_m(t) + \sigma_m {}^m P_{\rm in} - {}^m P_{\rm out} + \sigma_s D_s(t) \\ & + \sigma_s {}^s P_{\rm in} - {}^s P_{\rm out} + \\ & + u_{t_m} y_{t_m} + u_{t_s} y_{t_s} + F_h^T v_m + F_e^T v_s. \end{aligned} \tag{43}$$

Since the tanks and the robots are interconnected by means of the power preserving interconnection (38), we have that $F_i^T v_i = -u_{t_i} y_{t_i}$, where $i = m, s$, and therefore, (43) can be rewritten as

$$\begin{aligned} \dot{\mathcal{H}}(t) = & -(1-\sigma_m) D_m(t) - (1-\sigma_s) D_s(t) \\ & + \sigma_m {}^m P_{\rm in} - {}^m P_{\rm out} + \\ & + \sigma_s {}^s P_{\rm in} - {}^s P_{\rm out} + F_h^T v_m + F_e^T v_s. \end{aligned} \tag{44}$$

Using (40), we have that

$$\begin{aligned} \dot{\mathcal{H}}(t) = & -(1-\sigma_m) D_m(t) - (1-\sigma_s) D_s(t) \\ & - (1-\sigma_m) {}^s P_{\rm out} - \\ & - (1-\sigma_s) {}^m P_{\rm out} + F_h^T v_m + F_e^T v_s. \end{aligned} \tag{45}$$

Since $\sigma_i \in \{0, 1\}$ and since ${}^i P_{\rm out}, D_i \geq 0$ for $i = m, s$, it follows that

$$\dot{\mathcal{H}}(t) \leq F_h^T v_m + F_e^T v_s \tag{46}$$

which proves the statement. ■

Passivity guarantees a stable behavior of the teleoperation system during the compensation phase and while teleoperating the slave. If the exchange of energy between the tanks is not sufficient for guaranteeing a sufficient level of energy in the tanks, then it is necessary to augment the local damping of the robots. Intuitively, increasing the damping is a passivity preserving operation, and formally, passivity can be proven following the same lines of Proposition 2, using a variable damping matrix in the port-Hamiltonian models of master and slave.

The proposed teleoperation strategy is robust with respect to communication delay between master and slave since, as detailed in [10], the two layer approach preserves passivity in the delayed case.

VI. I-SUR Robot

The I-SUR robotic platform was designed with the aim of autonomously performing relatively simple surgical actions, such as puncturing and suturing. In the first prototype of the robot, a platform with eight DOFs was developed to automate the procedure of percutaneous needle insertion. This task requires a large workspace to properly position and orient the needle over the target area, a high end-effector positioning accuracy, and a stiff structure to guide the needle during insertion. For this purpose, the I-SUR robot adopts a macro/microunit architecture [38], [39]. A 4-DOF macrounit consisting of a linear delta robot [40] serves as a gross positioning unit. The parallel structure of the macrounit offers a rigid platform capable of carrying the weight of the microunit, while ensuring high position accuracy for needle placement and insertion. The microunit consists of a 4-DOF robotic arm with hybrid kinematics and holds the needle at its distal end. Three of the four DOFs are actuated remotely from the moving platform of the macrounit, while the needle can be rotated during insertion via a belt and pulley drive located behind the needle holder. The needle holder incorporates a six-axis force/torque sensor (ATI Nano 17, ATI Industrial Automation Inc., NC, USA) to measure interaction forces and torques during needle insertion. Position sensing is achieved through encoders located at the level of each actuator, and through potentiometers providing a redundant position measure for safety purposes. The same macro/microstructure, equipped with specific tools and an additional microunit, will be adopted to execute autonomous suturing.

The control implementation of the robot is hierarchically organized into two control layers: the low-level control and the high-level control. The low-level control of the I-SUR robot involves position and velocity control in a cascaded manner [41] at the joint level, as well as trajectory following. This layer is implemented in real-time LabVIEW 2013 (National Instruments, USA) running on a PC with an eight-core Intel i-7 (3.4-GHz) processor. While the joint/velocity control runs at 10 kHz on an integrated field-programmable gate array board, the trajectory following is performed at 2 kHz on the target PC. The end-effector position is computed by solving the combined kinematics of both the macro- and microunits independently. In addition to position and velocity control, software safety routines that monitor position, velocity, and motor current are implemented in the low-level controller. The high-level controller defines the end-effector trajectory for the needle insertion based on preoperative data. It further includes the interaction control scheme described in Section IV that runs on top of the implemented joint position control, which allows the robot to dynamically interact with the environment in a controlled and stable manner.

The I-SUR robotic platform is a kinematically redundant manipulator. However, we assume that the redundancy is addressed in the low-level control. Thus, the implementation of thebrk high-level control in the task space as described in Section IV is not affected by redundancy.

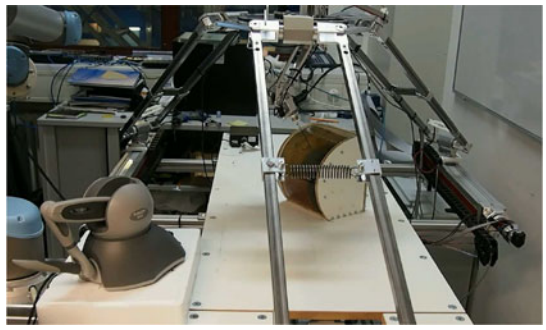

Fig. 4. Experimental setup used for validating the theoretical findings. The setup consists of the I-SUR robotic platform, a phantom of the human abdomen, and a PHANTOM OMNI haptic device.

VII. Experiments

We performed experimental tests on the semiautonomous robotic surgical system presented in Section VI in order to validate the theoretical findings presented in this paper. The accompanying video clip shows the experiment described in the following, while Fig. 4 shows the I-SUR robotic platform and the experimental setup. Further experiments can be found in [11], where a different robot was used to validate a strategy similar to the one presented in this paper.

The case study chosen to validate the control strategies is the insertion of needles through the skin since this is a task that requires high accuracy and reliability. The proposed experiment is only an example to illustrate the capabilities and a possible application of the overall methodology presented in this paper. The robot autonomously performs the insertion of the needle into a phantom of the human abdomen. The phantom includes artificial organs, produced using high-fidelity CAD models as described in [42], which are enclosed in a gelatin layer that replicates the features of human skin. While the needle penetrates the phantom, the occurrence of an undesired event is simulated: The needle is assumed to miss the target and then has to be extracted and reinserted under manual guidance (teleoperation). To this aim, when the occurrence of the event is detected, the system switches to the teleoperated mode and the user can manually extract the needle from the skin and correctly reinsert it. A PHANTOM OMNI haptic device was utilized as the master device of the teleoperation system. Since the orientation DOFs of the PHANTOM OMNI device are not actuated and, therefore, the reaction moments cannot be reflected to the user, the orientation is kept fixed when the system switches to the teleoperated mode. However, this practical limitation does not affect the generality of the approach described in Section V.

The control software was developed using the Orocos component-based framework [43] and includes, in addition to the computational components implementing the previously described control strategies, a motion task supervisor, implemented as a *reduced finite-state machine* module [44], a motion planner, which generates online collision-free paths in robot workspace coordinates using OMPL [45], communication

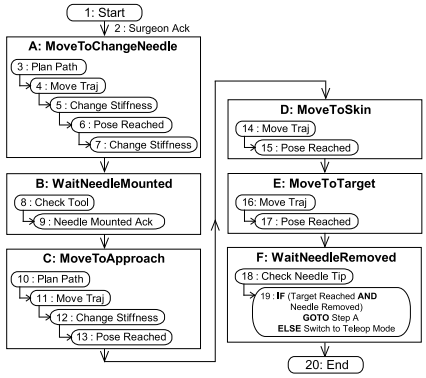

Fig. 5. Flowchart describing the robot activities executed during the experimental scenario. Letters and numbers, indicating the sequence of steps and operations, will be used to highlight interesting features of the experiment plots.

bridges toward the low-level robot controller, and a user interface interacting with the surgeon. The surgeon is, in fact, the primary driver of the surgical procedure, providing commands to proceed or interrupt the task execution sequence. In particular, the experimental scenario requires the robot to execute the activities described in the flowchart of Fig. 5. The main steps of the procedure are denoted using letters, while basic operations performed within each step are denoted using numbers. It is important to note that such letters and numbers will be used in the rest of the section to highlight interesting features of the experiment plots and relate them to the overall sequence of the task. The surgical procedure is started when the robot is in a *home* position, and the robot is then moved along a collision-free path (i.e., avoiding the phantom or any other obstacle in the workspace) generated online, to a position allowing the surgeon to mount the needle onto the end-effector. Because of strict tolerance settings in collision-checking algorithms, the path generation may require up to 15 s on the PC available in the experimental setup. Moreover, the system is required to await an acknowledgment from the surgeon, verifying the correct installation of the needle. Once the needle is mounted, the robot moves toward the final target in three steps: First, a collision-free path to an approach position is generated and executed; then, a sequence of two properly aligned linear trajectories of specified lengths are executed, without any collision checking, to get in contact with the skin and then penetrate it. The robot is finally stopped and waits for the removal of the needle from its end-effector.

A. Autonomous Needle Insertion

In this section, we will focus on the first part of the experiment, where the needle is autonomously inserted by the robot following the desired trajectory to reach a specific target inside the phantom. Thus, we will show the results of the implementation of the variable admittance control.

After many experimental evaluations, the inertial and damping parameters of the desired interaction model (16) were empirically chosen as the following constant diagonal matrices:

$$\Lambda_d = \text{diag}\{0.5, 0.5, 0.5, 0.01, 0.01, 0.01\} \quad [\text{kg}]$$
$$D_d = \text{diag}\{D_{d1}, D_{d2}\}$$

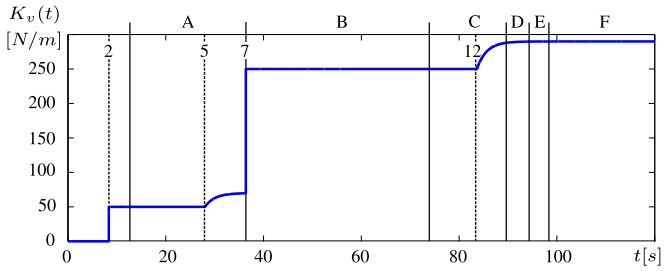

Fig. 6. Evolution over time of the values chosen as diagonal elements for the variable part of the stiffness matrix during the autonomous needle insertion. (The numbers and the letters refer to the steps and operations in Fig. 5.)

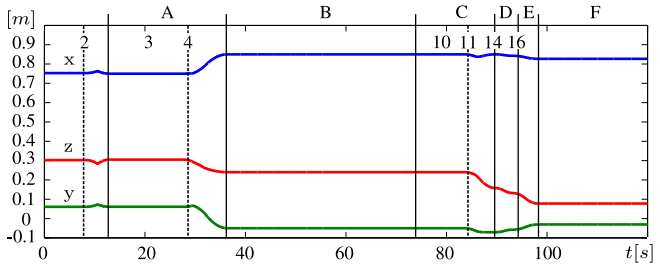

Fig. 7. Desired cartesian positions computed by the admittance controller. (The numbers and the letters refer to the steps and operations in Fig. 5.)

where

$$D_{d1} = \text{diag}\{50, 50, 50\} \quad [\text{N·s/m}]$$
$$D_{d2} = \text{diag}\{10, 10, 10\} \quad [\text{N·ms/rad}]\,.$$

Since during the puncturing task, the robot has to behave in different ways depending on the environment it has to interact with, the entries for the stiffness matrix change during the operation. Indeed, for example, the robot can be compliant while it is in free motion, while it has to be stiff for penetrating the skin. To preserve the clarity of the presentation, the following plots will show only the results regarding the translational coordinates x, y, and z. Similar results have been obtained for the rotational coordinates.

The evolution over time of the variable part $K_v(t)$ of the stiffness matrix is shown in Fig. 6, while the constant part is chosen as

$$K_c = \text{diag}\{K_{c1}, K_{c2}\}$$

where

$$K_{c1} = \text{diag}\{10, 10, 10\} \quad [\text{N/m}]$$
$$K_{c2} = \text{diag}\{10, 10, 10\} \quad [\text{N·m/rad}]\,.$$

To demonstrate that the system remains stable despite the stiffness changes, we even consider different ways of varying the stiffness profile. For example, during the movement of the robot to the position of needle change, the stiffness is augmented gradually, whereas when the robot is waiting for the needle to be mounted, the stiffness is changed instantly.

The desired Cartesian translational positions computed by the admittance controller are reported in Fig. 7. As expected, the commanded motion does not diverge over time, and the system

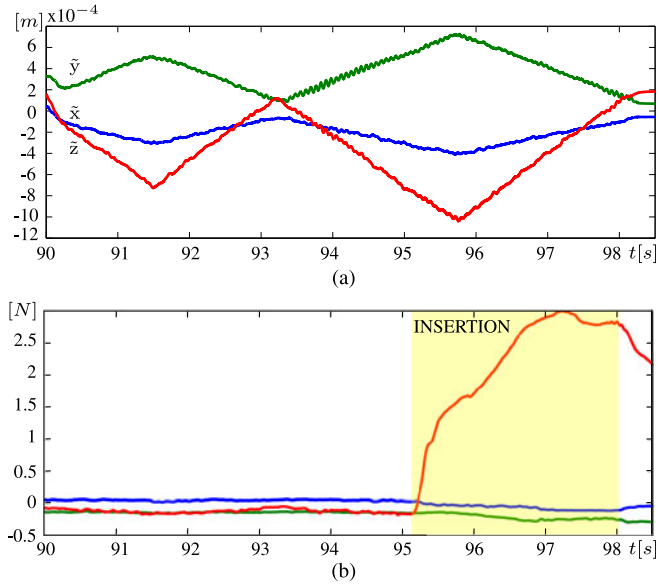

Fig. 8. Tracking error (i.e., difference between the position of the robot end-effector and the desired trajectory) and measured forces during the approach and insertion phases. (a) Tracking error. (b) Measured forces.

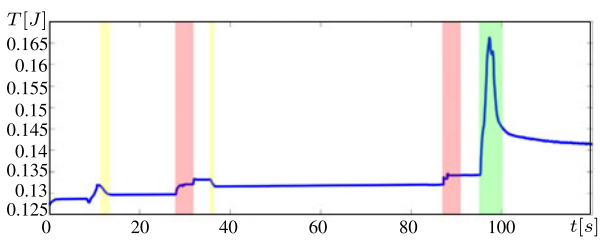

Fig. 9. Evolution over time of the energy level of the tank during the autonomous insertion. Yellow regions correspond to instantaneous variations of stiffness, while red areas correspond to gradual changes of stiffness. The green region highlights the evolution of the tank energy during the motion of the needle inside the phantom.

remains stable despite the many changes of stiffness. Fig. 8(a) shows that the tracking error during the insertion of the needle (phase E) is below the acceptable value of 0.0011 m, thanks to the high values of the stiffness in this phase, while Fig. 8(b) shows the forces measured during the same time interval.

Fig. 9 shows the behavior of the tank energy T. The energy thresholds are chosen as $\bar{T} = 10$ J and $\varepsilon = 0.1$ J. When the stiffness changes instantly, at $t = 10$ s and $t = 36$ s (yellow regions in Fig. 9), the required energy to implement this behavior is extracted from the tank. On the other hand, the gradual changes of stiffness, red areas at $t = 28$ s and $t = 83.5$ s, are dissipative actions, and thus, the tank energy rises. The energy level has a big increment when the needle penetrates the skin ($t = 93$ s) since this action is dissipative, but then, during the motion of the needle inside the phantom, the tank is emptied again to perform the movement, and the tank energy decreases accordingly (green region). Little energy is extracted or inserted into the tank because, as shown, for example, in Fig. 8(a), the trajectory error $\tilde{x}(t)$ is small, and then, from (24), the values of $w(t)$ used in (23) are small too.

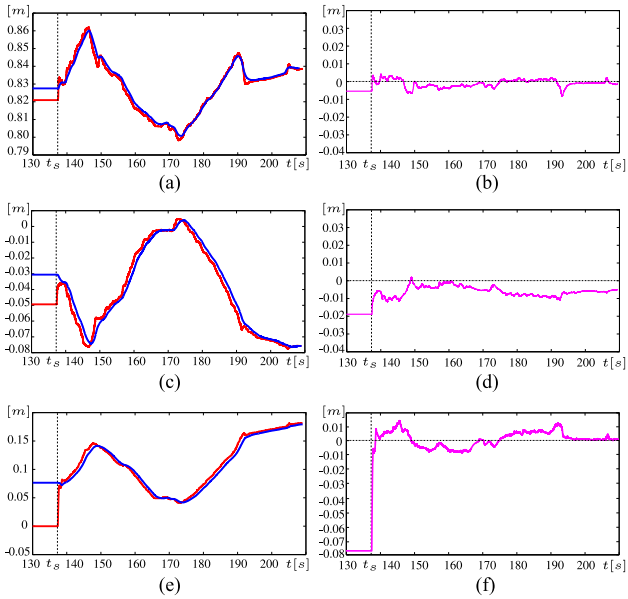

Fig. 10. Cartesian positions of master (red lines) and slave (blue lines) during the teleoperation phase. At the switching instant t_s, master and slave are not aligned, while, after a short transient, the coupling between the two motions becomes effective. The plots on the right show the position errors between master and slave (a) x_m (red) and x_s (blue) (b) $x_m - x_s$ (c) y_m (red) and y_s (blue) (d) $y_m - y_s$ (e) z_m (red) and z_s (blue) (f) $z_m - z_s$.

B. Switching to Teleoperation for Manual Needle Extraction and Reinsertion

In this section, we will take into account the second part of the experiment: The needle has been autonomously inserted, but due to an unexpected event, the target is missed. The system recognizes this event and switches to teleoperation. The switching instant is $t_s = 137.3$ s.

According to the theory developed in the previous sections, the following design choices were made.

1) The control parameters in Fig. 2 are $K = 50$ N/m, $B = 1.1$ N·s/m, $R_m = R_s = 5$ N·s/m.
2) The following values for the energy thresholds have been selected: $\bar{T}_i = 20$ J, ${}^iT_{\text{ava}} = 10$ J, ${}^iT_{\text{req}} = 5$ J, $\varepsilon_i = 1$ J, where $i = m, s$.
3) The nonincreasing functions $f_1(e(t))$ and $f_2(\lambda(t))$ in (35) and (36) are defined as

$$f_1(e(t)) = \frac{1}{2}\left[\cos\left(\pi\frac{e(t) - \bar{e}_1}{\bar{e}_1}\right) + 1\right] \quad (47)$$

$$f_2(\lambda(t)) = \frac{1}{2}\left[\cos\left(\pi\frac{\lambda(t) - \bar{\lambda}_1}{\bar{\lambda}_1}\right) + 1\right]. \quad (48)$$

With this choice, the functions smoothly change from 0 (when $e(t) = \bar{e}_2$ and $\lambda(t) = \bar{\lambda}_2$) to 1 (when $e(t) = \bar{e}_1$ and $\lambda(t) = \bar{\lambda}_1$), with $\bar{e}_1 = \frac{\bar{e}_2}{2}$ and $\bar{\lambda}_1 = \frac{\bar{\lambda}_2}{2}$. Indeed, the cosine is a continuous function that allows smooth transitions between the two values, while avoiding abrupt variations.
4) The thresholds related to the functions $\alpha_1(e(t))$ and $\alpha_2(\lambda(t))$ are chosen as $\bar{e}_1 = 0.005$ m, $\bar{e}_2 = 0.01$ m, $\bar{\lambda}_1 = 0.005$ m, and $\bar{\lambda}_2 = 0.01$ m. Such small values are justified by the surgical context, prescribing that the bilateral

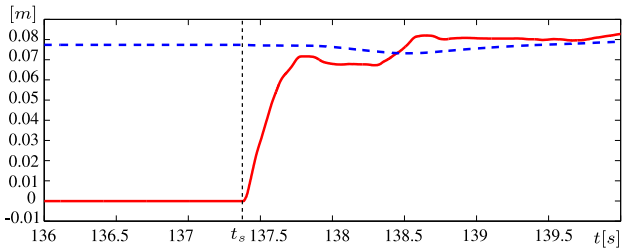

Fig. 11. Detail of the z coordinate of master (red solid line) and slave (blue dashed line) cartesian position during the transient. At the switching instant t_s, master and slave are not aligned. Then, the master starts moving toward the slave position, and at the end of the alignment phase, the teleoperation is completely operative and master and slave are fully coupled.

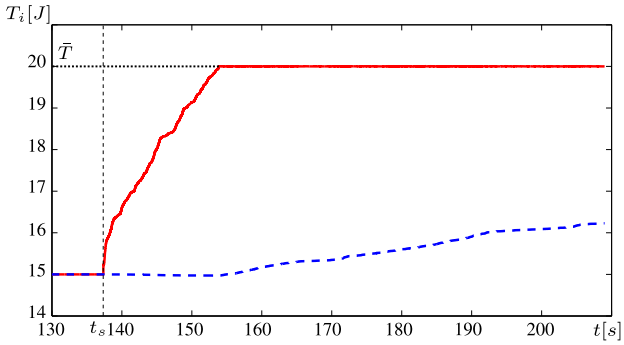

Fig. 12. Energy level of the tanks at the master (red solid line) and slave (blue dashed line) sides when the teleoperation mode is active.

interconnection is only enabled when the mismatch between master and slave is small. In case of less critical tasks, larger tolerances could be chosen.

In Fig. 10, we show the Cartesian positions of master and slave and the position errors, while Fig. 11 shows the detail of the z coordinate of master and slave positions during the alignment transient. As shown in Fig. 10, at the switching instant, master and slave are not aligned, and the following pose offsets arise when teleoperation is switched ON:

$$\begin{aligned} L_x(t_s) &= \mathrm{x_m}(t_s) - \mathrm{x_s}(t_s) = -0.006 \text{ m} \\ L_y(t_s) &= \mathrm{y_m}(t_s) - \mathrm{y_s}(t_s) = -0.01866 \text{ m} \\ L_z(t_s) &= \mathrm{z_m}(t_s) - \mathrm{z_s}(t_s) = -0.07735 \text{ m}. \end{aligned}$$

According to the method described in Section V, the rest length L is replaced by the continuous time function $l(t)$ whose initial value is given by L, but at the end of the compensation, its result is equal to 0. At the switching instant, the operator feels a force guiding him/her to align the master position with the slave position. At the same time, the functions $\alpha_1(e(t))$ and $\alpha_2(\lambda(t))$ defined in (35) and (36) increase, because $l(t)$ and the misalignment decrease, respectively. The force due to the bilateral coupling is applied to the slave device weighted by $\alpha_1\alpha_2$. This means that the slave would not move until α_1 and α_2 will be close to one.

At the end of the alignment phase, we have $\alpha_1 = \alpha_2 = 1$. This means that the teleoperation is completely operative, and master and slave are fully coupled. Indeed, as shown in Fig. 11, the slave starts moving only when the master position is very close to the slave position, i.e., the distance between master and slave is below the threshold of 0.01 m, and the coupling between the two motions becomes effective. As master and slave are interconnected by using the coupling in (33), the forces felt at the master side are proportional to the position error between master and slave. Thanks to the action of the variable rest length, the forces gradually decrease from the initial value, and this results in a smooth behavior.

Fig. 12 shows the energy level of the tanks at the master and slave sides. It can be seen that the master stores energy until it reaches the upper bound $\bar{T}$ around $t = 154$ s. The energy not stored in the tank is then sent to the slave tank, which increases its level faster than before. Thanks to the exchange of energy between master and slave tanks, the energy in the tanks is well distributed, and it was never required to augment the damping during our experiments to keep the filling level of the tanks high enough, as shown in Fig. 12. Nevertheless, if further energy were necessary for refilling the tanks, a local damping injection [8] can be activated. In order to avoid asymmetry in the viscous force felt by the user, the damping should be isotropic, and consequently, the control action distributed in all directions.

This test shows that the exchange of energy during the alignment and the normal teleoperation works as expected.

It is worth noting that, during the transition from the "locked" slave robot to the teleoperated slave robot, there are no spikes, oscillations, or abrupt movements. The proposed control architecture allows to switch from fully autonomous mode to teleoperated mode in a stable manner, which is essential for critical applications such as robotic surgery.

VIII. Conclusion

Autonomous surgical systems in soft tissue surgery are still in a very preliminary conceptual phase. As they progress, they will be useful in the operating room to allow the surgeon to focus only on the most critical parts of the surgical procedure. Since in soft tissue surgery, the robot has to interact with environments mostly unknown and usually deformable, the control of the interaction behavior of the robot is fundamental. Furthermore, it might happen that the autonomous system cannot complete the procedure due to unexpected events. In this case, the intervention of the surgeon is mandatory, and the transition from autonomous mode to teleoperated mode has to be carefully managed to avoid abrupt movements and oscillations that could harm the patient.

In this study, we proposed an admittance control strategy characterized by a time-varying stiffness, damping, and inertia to assure passivity during interaction with the human body. By properly controlling the energy exchanged during the action, the system is guaranteed to be passive for any choice of the stiffness and inertia matrices. Therefore, the robot exhibits stable behavior, both in free motion and in interaction with partially unknown environments (e.g., the body of the patient).

Moreover, we proposed a stable, reliable, and accurate procedure to handle the challenging transition phase between autonomous mode and teleoperation of a surgical robot. Indeed, abrupt forces due to the switch have been avoided, especially those applied to the slave robot, and the kinematic mismatch

is progressively reduced so that the accuracy is increased. Finally, since the overall teleoperation system has been formally proven to be passive, stability and reliability are guaranteed. The proposed control architecture is based on a two-layer bilateral control architecture that guarantees stability and smooth variation of the critical variables. The freedom in the choice of control parameters and functions can be exploited to adapt the proposed solution to different conditions. The proposed architecture has been implemented on a semiautonomous robotic surgical system designed within the I-SUR project, and the results of related experiments have been discussed. The techniques developed in the paper are general, and they can be extended to other more complex automated surgical scenarios where a robot has to interact with a soft tissue and where a switch between autonomous mode and teleoperation mode is necessary.

Future work aims at selecting a proper stiffness profile that reflects an online estimation of the environmental stiffness. Furthermore, it has to be investigated how the energy extracted from the tank can be modulated when its filling level is close to the minimum (i.e., degraded operating mode). The methodologies presented in this paper ensure stability of the system, which is a necessary prerequisite for safety in robotic surgery. However, to make the procedure completely safe for the patient, other higher level safety measures must be in place to monitor the proper execution of the task.

REFERENCES

[1] Intuitive Surgical. (2015). [Online]. Available: http://www.intuitivesurgical.com.

[2] A. Tobergte, R. Konietschke, and G. Hirzinger, "Planning and control of a teleoperation system for research in minimally invasive robotic surgery," in *Proc. IEEE Int. Conf. Robot. Autom.*, Kobe, Japan, May 2009, pp. 4225–4232.

[3] G. P. Moustris, S. C. Hiridis, K. M. Deliparaschos, and K. M. Konstantinidis, "Evolution of autonomous and semi-autonomous robotic surgical systems: A review of the literature," *Int. J. Med. Robot. Comput. Assisted Surgery*, vol. 7, no. 4, pp. 375–392, 2011.

[4] M. Bonfe, F. Boriero, R. Dodi, P. Fiorini, A. Morandi, R. Muradore, L. Pasquale, A. Sanna, and C. Secchi, "Towards automated surgical robotics: A requirements engineering approach," in *Proc. IEEE RAS EMBS Int. Conf. Biomed. Robot. Biomechatron.*, 2012, pp. 56–61.

[5] N. Hogan, "Impedance control: An approach to manipulation. I—Theory. II—Implementation. III—Applications," *ASME J. Dyn. Syst. Meas. Control*, vol. 107, pp. 1–24, 1985.

[6] B. Hannaford, "Stability and performance tradeoffs in bi-lateral telemanipulation," in *Proc. IEEE Int. Conf. Robot. Autom.*, Scottsdale, AZ, USA, May 1989, pp. 1764–1767.

[7] P. F. Hokayem and M. W. Spong, "Bilateral teleoperation: An historical survey," *Automatica*, vol. 42, no. 12, pp. 2035–2057, 2006.

[8] C. Secchi, S. Stramigioli, and C. Fantuzzi, *Control of Interactive Robotic Interfaces: A Port-Hamiltonian Approach* (ser. Springer Tracts in Advanced Robotics), vol. 29. New York, NY, USA: Springer-Verlag, 2006.

[9] C. Secchi, S. Stramigioli, and C. Fantuzzi, "Position drift compensation in port-hamiltonian based telemanipulation," in *Proc. IEEE/RSJ Int. Conf. Intell. Robots Syst.*, 2006, pp. 4211–4216.

[10] M. Franken, S. Stramigioli, S. Misra, C. Secchi, and A. Macchelli, "Bilateral telemanipulation with time delays: A two-layer approach combining passivity and transparency," *IEEE Trans. Robot.*, vol. 27, no. 4, pp. 741–756, Aug. 2011.

[11] F. Ferraguti, C. Secchi, and C. Fantuzzi, "A tank-based approach to impedance control with variable stiffness," presented at the IEEE Int. Conf. Robot. Automat., Karlsruhe, Germany, May 2013.

[12] P. Fiorini, R. Muradore, G. Akgun, D. E. Barkana, M. Bonfè, F. Boriero, G. De Rossi, R. Dodi, O. J. Elle, F. Ferraguti, L. Gasperotti, R. Gassert, K. Mathiassen, D. Handini, O. Lambercy, L. Li, M. Kruusma, A. Manurung, G. Meruzzi, P. Nguyen, N. Preda, A. Ristolainen, A. Sanna, C. Secchi, and A. E. Yantac, "Development of a cognitive robotic system for simple surgical tasks," *Int. J. Adv. Robot. Syst.*, vol. 12, no. 37, pp. 1–20, 2015.

[13] J. Buchli, E. Theodorou, F. Stulp, and S. Schaal, "Variable impedance control: A reinforcement learning approach," presented at the Robot.: Sci. Syst. Conf., Zaragoza, Spain, Jun. 2010.

[14] T. Tsumugiwa, R. Yokogawa, and K. Hara, "Variable impedance control based on estimation of human arm stiffness for human-robot cooperative calligraphic task," presented at the IEEE Int. Conf. Robot. Autom., Washington, DC, USA, May 2002.

[15] W. Zarrad, P. Poignet, R. Cortesão, and O. Company, "Towards teleoperated needle insertion with haptic feedback controller," in *Proc. IEEE/RSJ Int. Conf. Intell. Robots Syst.*, 2007, pp. 1254–1259.

[16] J. H. Park and H. C. Cho, "Impedance control with varying stiffness for parallel-link manipulators," presented at the Am. Control Conf., Philadelphia, PA, USA, Jun. 1998.

[17] C. Yang, G. Ganesh, S. Haddadin, S. Parusel, A. Albu-Schäffer, and E. Burdet, "Human-like adaptation of force and impedance in stable and unstable interactions," *IEEE Trans. Robot.*, vol. 27, no. 5, pp. 918–930, Oct. 2011.

[18] G. Ganesh, N. Jarrasé, S. Haddadin, A. Albu-Schäffer, and E. Burdet, "A versatile biomimetic controller for contact tooling and haptic exploration," in *Proc. IEEE Int. Conf. Robot. Autom.*, Saint Paul, MN, USA, May 2012, pp. 3329–3334.

[19] K. Lee and M. Buss, "Force tracking impedance control with variable target stiffness," in *Proc. Int. Federation Automat. Control World Congr.*, Seoul, Korea, Jul. 2008, pp. 6751–6756.

[20] X. Zhang and O. Ivlev, "Simulation of interaction tasks for pneumatic soft robots using SimMechanics," in *Proc. IEEE Int. Workshop Robot. Alpe–Adria–Danube Region*, Budapest, Hungary, Jun. 2010, pp. 149–154.

[21] M. Kordasz, K. Kuczkowski, and P. Sauer, "Study on possible control algorithms for lower limb rehabilitation system," presented at the IEEE Int. Conf. Rehabil. Robot., Zurich, Switzerland, Jul. 2011.

[22] J. Feio, J. M. Martins, and J. Sá da Costa, "Variable impedance control of manipulator robots applied to orthopedic surgery," in *Proc. 7th Workshop Adv. Control Diagnosis*, Zielona Gra, Poland, Nov. 2009.

[23] R. Anderson, "Autonomous, teleoperated, and shared control of robot systems," in *Proc. IEEE Int. Conf. Robot. Autom.*, 1996, pp. 2025–2032.

[24] H. Baier, M. Buss, and G. Schmidt, "Control mode switching for teledrilling based on a hybrid system model," in *Proc. IEEE/ASME Int. Conf. Adv. Intell. Mechatron.*, 1997, p. 50.

[25] Y. Yokokohji, A. Ogawa, H. Hasunuma, and T. Yoshikawa, "Operation modes for cooperating with autonomous functions in intelligent teleoperation systems," in *Proc. IEEE Int. Workshop Robot Human Commun.*, 1992, pp. 275–281.

[26] P. Xiong, A. Song, K. Qian, L. Zhang, and X. Xu, "Operation modes and control schemes for a telerobot with time delay," *Int. J. Adv. Robot. Syst.*, vol. 9, no. 57, pp. 1–8, 2012.

[27] C. Secchi, S. Stramigioli, and C. Fantuzzi, "Compensation of position errors in passivity based teleoperation over packet switched communication networks," presented at the *IFAC World Congr.*, Seoul, Korea, Jul. 2008.

[28] A. F. Villaverde, A. Barreiro, and C. Raimúndez, "Passive position error correction in internet-based teleoperation," *Automatica*, vol. 46, no. 11, pp. 1884–1890, 2010.

[29] J. Artigas, J. H. Ryu, and C. Preusche, "Position drift compensation in time domain passivity based teleoperation," in *Proc. IEEE/RSJ Int. Conf. Intell. Robots Syst.*, Taipei, Taiwan, Oct. 2010, pp. 4250–4256.

[30] A. Franchi, C. Secchi, H. I. Son, H. H. Bülthoff, and P. R. Giordano, "Bilateral teleoperation of groups of mobile robots with time-varying topology," *IEEE Trans. Robot.*, vol. 28, no. 5, pp. 1019–1033, Oct. 2012.

[31] P. R. Giordano, A. Franchi, C. Secchi, and H. H. Bülthoff, "A passivity-based decentralized strategy for generalized connectivity maintenance," *Int. J. Robot. Res.*, vol. 32, no. 3, pp. 299–323, 2013.

[32] D. Lee and K. Huang, "Passive-set-position-modulation framework for interactive robotic systems," *IEEE Trans. Robot.*, vol. 26, no. 2, pp. 354–369, Apr. 2010.

[33] L. Villani and J. De Schutter, "Force control," in *Springer Handbook of Robotics*, B. Siciliano and O. Khatib, Eds. Berlin, Germany: Springer, 2008, ch. 7.

[34] L. Barbé, B. Bayle, M. de Mathelin, and A. Gangi, "Online robust model estimation and haptic clues detection during in vivo needle insertions," in *Proc. 1st IEEE/RAS-EMBS Int. Conf. Biomed. Robot. Biomechatron.*, Feb. 2006, pp. 341–346.

[35] E. Nuno, R. Ortega, N. Barabanov, and L. Basanez, "A globally stable PD controller for bilateral teleoperators," *IEEE Trans. Robot.*, vol. 24, no. 3, pp. 753–758, Jun. 2008.

[36] D. Lee and M. W. Spong, "Passive bilateral teleoperation with constant time delay," *IEEE Trans. Robot.*, vol. 22, no. 2, pp. 269–281, Apr. 2006.
[37] C. Secchi, A. Franchi, H. H. Bülthoff, and P. R. Giordano, "Bilateral teleoperation of a group of UAVs with communication delays and switching topology," in *Proc. IEEE Int. Conf. Robot. Autom.*, Saint Paul, MN, USA, May 2012, pp. 4307–4314.
[38] O. Khatib, "Inertial properties in robotic manipulation: An object-level framework," *Int. J. Robot. Res.*, vol. 14, pp. 19–36, Feb. 1995.
[39] O. Khatib, "Reduced effective inertia in macro-/mini-manipulator systems," in *Proc. Int. Symp. Robot. Res.*, 1991, pp. 279–284.
[40] M. Bouri and R. Clavel, "The linear delta: Developments and applications," in *Proc. Int. Symp. Robot. German Conf. Robot.*, Munich, Germany, Jun. 2010, pp. 1198–1205.
[41] R. Franks and C. Worley, "Quantitative analysis of cascade control," *Ind. Eng. Chem.*, vol. 48, no. 6, pp. 1074–1079, Jun. 1956.
[42] R. Opik, A. Hunt, A. Ristolainen, P. M. Aubin, and M. Kruusmaa, "Development of high fidelity liver and kidney phantom organs for use with robotic surgical systems," in *Proc. IEEE/RAS EMBS Int. Conf. Biomed. Robot. Biomechatron.*, Rome, Italy, Jun. 2012, pp. 425–430.
[43] The Orocos Project. (2015). [Online]. Available: http://www.orocos.org.
[44] M. Klotzbücher and H. Bruyninckx, "Coordinating robotic tasks and systems with rFSM statecharts," *J. Softw. Eng. Robot.*, vol. 3, no. 1, pp. 28–56, Jan. 2012.
[45] Open Motion Planning Library. (2015). [Online]. Available: http://ompl.kavrakilab.org.

Federica Ferraguti (S'13–M'15) received the M.Sc. degree in industrial and management engineering and the Ph.D. degree in industrial innovation engineering from University of Modena and Reggio Emilia, Modena, Italy, in 2011 and 2015, respectively.

She was a Visiting Student with the Rehabilitation Engineering Laboratory, ETH Zurich, Zurich, Switzerland, in 2013. She is currently a Postdoctoral Research Fellow with University of Modena and Reggio Emilia. Her research interests include surgical robotics, telerobotics, control of robotic systems, and human–robot physical interaction.

Nicola Preda received the M.Sc. and Ph.D. degrees in automation engineering from University of Ferrara, Ferrara, Italy, in 2011 and 2015, respectively.

He is a Postdoctoral Research Fellow with the Department of Engineering, University of Ferrara. His research interests include system and software architecture, software engineering, and control of robotic systems.

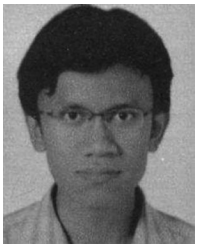

Auralius Manurung (S'10) received the M.Sc. degree from School of Mechanical and Aerospace Engineering, Gyeongsang National University, Jinju, Korea, in 2011.

He joined the Rehabilitation Engineering Laboratory, ETH Zurich, Zurich, Switzerland, in September 2011 for Ph.D. research. His research interests include the area of design and control of robotic systems for biomedical applications.

Marcello Bonfè (M'02) received the M.Sc. degree in electronic engineering from University of Ferrara, Ferrara, Italy, in 1998 and the Ph.D. in information engineering from University of Modena and Reggio Emilia, Modena, Italy, in 2003.

He is an Assistant Professor of automatic control with University of Ferrara, Ferrara, Italy. He has published more than 70 refereed journal and conference papers. His main research interests include formal verification of discrete event systems, modeling and control of mechatronic systems, fault detection and fault-tolerant control, robotics, and motion planning.

Olivier Lambercy (S'06–M'10) received the M.Sc. degree in microengineering from Ecole Polytechnique Fédérale de Lausanne, Lausanne, Switzerland, in 2005 and the Ph.D. degree in mechanical engineering from National University of Singapore, Singapore, in 2009.

His main contributions are in the field of robot-assisted rehabilitation and assessment of hand function after stroke. Since 2009, he has been a Research Associate with the Rehabilitation Engineering Laboratory, ETH Zurich, Zurich, Switzerland. His main research interests include medical and rehabilitation robotics, motor control, and human–machine interaction.

Roger Gassert (S'02–M'06–SM'13) received the M.Sc. degree in microengineering and the Ph.D. degree in neuroscience robotics from Ecole Polytechnique Fédérale de Lausanne, Lausanne, Switzerland, in 2002 and 2006, respectively.

Since 2008, he has been an Assistant Professor and, since 2014, an Associate Professor of rehabilitation engineering with ETH Zurich, Zurich, Switzerland. He has made contributions to the field of neuroscience robotics to investigate sensorimotor control and related dysfunctions, as well as to robot-assisted assessment and therapy. His research interests include physical human–machine interaction, rehabilitation and medical robotics, assistive technology, and the neural control of movement.

Riccardo Muradore (S'99–M'04) received the Laurea degree in information engineering and the Ph.D. degree in electronic and information engineering from University of Padova, Padova, Italy, in 1999 and 2003, respectively.

He was a Postdoctoral Fellow with the Department of Chemical Engineering, University of Padova, from 2003 to 2005. He then spent three years with the European Southern Observatory, Munich, Germany, as a Control Engineer working on adaptive optics systems. In 2008, he joined the ALTAIR Robotics Laboratory, University of Verona, Verona, Italy, where he has been an Assistant Professor since 2013. His research interests include robust control, teleoperation, robotics, networked control systems, and adaptive optics.

Paolo Fiorini (F'09) received the Laurea degree in electronic engineering from University of Padova, Padova, Italy; the M.S.E.E. degree from University of California at Irvine, Irvine, CA, USA; and the Ph.D. degree in mechanical engineering from University of California, Los Angeles, CA, USA.

From 1985 to 2000, he was with NASA Jet Propulsion Laboratory, California Institute of Technology, where he worked on telerobotic and teloperated systems for space exploration. From 2000 to 2009, he was an Associate Professor of control systems with the School of Science, University of Verona, Verona, Italy, where he founded the ALTAIR Robotics Laboratory with his students. He is currently a Full Professor of computer science with the University of Verona. His research focuses on teleoperation for surgery, service, and exploration robotics funded by several European Projects.

Cristian Secchi (M'04) received the M.Sc. degree in computer science engineering from University of Bologna, Bologna, Italy, in 2000. He received the Ph.D. degree in information engineering from University of Modena and Reggio Emilia, Modena, Italy, in 2004.

He is an Associate Professor with the University of Modena and Reggio Emilia.

Dr. Secchi's Ph.D. thesis was selected as one of the three finalists of the 5th Georges Giralt Award for the best Ph.D. thesis on robotics in Europe. He participated to the CROW project, selected as one of the finalists for the 2010 EUROP/EURON Technology Transfer Award for the Best Technology Transfer Project in Europe. He is an Associate Editor for *IEEE Robotics and Automation Magazine* and he is currently an Associate Editor of IEEE TRANSACTIONS ON ROBOTICS and of IEEE ROBOTICS AND AUTOMATION LETTERS. His research interests include human–robot physical interaction, telerobotics, mobile robotics, and surgical robotics. He has published more than 100 papers on international journals and conferences.